HTML ABSTRACT + LINKS

Pulsed laser-deposited single-crystal LiZn-ferrite films with low microwave loss

Young-Yeal Song,[a] Michael S. Grinolds, Pavol Krivosik,[b] and Carl E. Patton
Department of Physics, Colorado State University, Fort Collins, Colorado 80523

(Received 8 December 2004; accepted 7 March 2005; published online 6 May 2005)

Lithium zinc ferrite (LiZnF) films were prepared for a wide range of deposition parameters. Bulk LiZnF rather than pure Li ferrite targets were used to mediate the mismatch problem between the film and the MgO substrate. Preparation conditions were optimized to give single phase epitaxial films with half power ferromagnetic-resonance (FMR) linewidths of as low as 57 Oe at 9.5 GHz. The films were deposited on (100)-plane MgO substrates with a KrF excimer laser at a wavelength of 248 nm. The minimum linewidth films with a thickness of 0.70 μm were obtained for an oxygen partial pressure of 400 mTorr, a substrate temperature of 800 °C, and a laser fluence of 1.7 J/cm^2. X-ray diffraction pattern indicated a pure LiZn phase with local normal axis deviations below 0.05°. The FMR profiles were measured at 9.5 GHz with the static field perpendicular and parallel to the film plane, and as a function of rotation angle for in-plane fields. The data yielded a saturation induction $4\pi M_s$ value of 2.730 kG, about the same as for a bulk, and cubic anisotropy, with a first-order cubic anisotropy energy constant K_1 of about 7.33×10^3 ergs/cm^3, a factor of five or smaller than that for a bulk LiZn ferrite. © *2005 American Institute of Physics*.
[DOI: 10.1063/1.1897833]

I. INTRODUCTION

Lithium ferrite (Li-ferrite) is an attractive material for microwave applications because of its relatively high magnetization, small loss tangent, and the range of modifications possible through zinc and other substitutions.[1–4] There are also potential applications of lithium ferrite thin films for planar microwave devices. Such applications, however, require materials with low microwave loss and small ferromagnetic-resonance (FMR) linewidths. Oliver *et al.*[5] and Balestrino *et al.*[6] have produced Li-ferrite films by pulsed laser deposition (PLD) with *X*-band half power FMR linewidths in the 200–400-Oe range. Such linewidths are more than a factor of 100–200 larger than obtained for bulk single crystals.[7,8] Much lower losses are required for lithium ferrite films to be a useful option for thin-film microwave applications.

The objective of this work was to develop low microwave loss Li-ferrite thin films by PLD processes and improve on the properties reported by previous workers. The approach was to (a) optimize the PLD deposition parameters as much as possible based on previous successes for barium ferrite PLD films,[9] and (b) take advantage of zinc substitutions to provide a better lattice match with MgO substrates. Modest zinc substitutions of up to 0.1 at./f.u. were used in Refs. 5 and 6 for an improved lattice match. Here, Li-ferrite target materials with Zn additions of 0.6 at./f.u. were used. For pure lithium ferrite, the lattice parameter is 1.15% less than twice the lattice parameter of MgO.[10] At 0.6 Zn at./f.u., the lattice mismatch can be reduced by a factor of four, down to 0.26%. Although this is still much higher than the lattice mismatch between yttrium iron garnet (YIG) and the standard gadolinium gallium garnet substrates used for the production of low linewidth YIG films, the substantial reduction in mismatch should allow for smaller linewidths than previously possible in Li-ferrite films.

The results demonstrate that one can produce good epitaxial Zn-substituted PLD films of lithium ferrite with substantially lower FMR linewidths than that reported up to now. The sample with the lowest loss had a thickness of 0.70 μm and half power FMR linewidth of 57 Oe at 9.5 GHz. Atomic force microscopy (AFM) analysis showed a very small surface roughness in the 0.3-nm range. The x-ray diffraction (XRD) pattern showed a spinel cubic structure with an extremely low crystallite orientation angular dispersion on the order of a few hundredths of a degree.

Section II describes the PLD sample preparation procedure and gives the conditions that were used to produce optimum low loss films. Section III gives the results on the film characterization and static magnetic properties. Section IV presents the FMR results, including the (a) linewidth data and the (b) FMR field versus angle data and a corresponding analysis of the magnetocrystalline anisotropy. Section V provides a summary.

II. FILM PREPARATION DETAILS

A pulsed excimer laser was used to ablate material from a target onto a substrate in a vacuum chamber with controlled atmosphere following standard PLD methods. The base vacuum pressure in the chamber was 2.3×10^{-7} Torr. A 99.999% pure oxygen fill was used for the depositions. The ablation was done with a KrF excimer laser at a wavelength of 248 nm and a stable single pulse energy held to 1.7 J/cm^2 ±1%. The focused beam had an estimated spot size on the

[a]Present address: Department of Physics, Chungbuk National University, Cheongju 361-763, Korea.
[b]On leave from the Faculty of Electrical Engineering and Information Technology, Slovak University of Technology, Bratislava, Slovakia.

 © 2005 American Institute of Physics

Downloaded 07 Jul 2005 to 129.82.140.121. Redistribution subject to AIP license or copyright, see http://jap.aip.org/jap/copyright.jsp

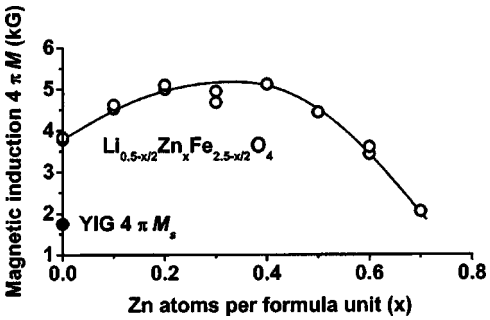

FIG. 1. Magnetic induction $4\pi M$ vs Zn content x in at./f.u. in polycrystalline $Li_{0.5-x/2}Zn_xFe_{2.5-x/2}O_4$, as measured on spherical samples at 8 kOe and room temperature. The solid line through the data points is a guide for the eye only. The solid dot at $x=0$ indicates the saturation induction of yttrium iron garnet (YIG) as a point of reference (see Ref. 15).

TABLE I. Summary of pulse laser deposition and other control parameters and conditions for the optimum linewidth lithium zinc ferrite films.

Parameter/condition	Value or description
Sample-target separation distance	4 cm
Laser pulse repetition rate (pulse/s)	1 (first minute) 3 (second minute) 5 (third minute) 10 (remaining time)
Substrate temperature	800 °C
Substrate material	(100)-oriented MgO
Oxygen partial pressure	400 mTorr
Deposition time	7 min
Postdeposition cooling rate	5 °C/min
Postdeposition atmosphere during cooling	High-Purity oxygen at 400 Torr

target of about 0.1 cm^2. The beam was rastered over the target through the use of a programmable mirror at a rate of 10 Hz. The target was also rotated at 15 rpm. The target was a 1/2-in.-diameter, 1/4-in.-thick $Li_{0.2}Zn_{0.6}Fe_{2.2}O_4$ disk produced by Trans Tech., Inc. by standard sintering techniques. The substrates were (100)-plane-oriented 5×5 mm^2 squares of 0.5-mm-thick MgO obtained from the MTI Corporation.

As indicated above, a lithium ferrite target with a zinc content of 0.6 at./f.u. was used for this work. As discussed in the introduction, the rationale for the use of zinc-substituted Li-ferrite is in the reduction in the lattice mismatch with the MgO substrate. The specific choice of 0.6 at./f.u. represents a trade off. Figure 1 shows the data on the room-temperature magnetic induction as a function of the Zn content x for the $Li_{0.5-x/2}Zn_xFe_{2.5-x/2}O_4$ (LiZnF) system. These data were obtained on spherical samples fabricated from conventionally sintered LiZn-ferrite materials by Trans Tech., Inc. The applied field for the measurements was 8 kOe. The figure also shows the room-temperature saturation induction for YIG for reference. These data show the well-established effect of zinc substitutions in increasing the magnetization for values of x below about 0.3–0.4.[4] For higher levels of Zn, there is a drop in the magnetization due to spin canting effects.[3,4] For $x=0.6$, the magnetization is still reasonably high and is still close to the value for pure Li-ferrite with no zinc. Smaller x values would yield a higher magnetization but a reduced advantage in terms of the lattice match. For larger x values, the substantial degradation in the magnetization and the noncollinear spin order associated with canting yields less than the desirable properties for microwave applications. The control parameters for the depositions were (1) the sample-target separation distance, (2) the laser pulse repetition rate, (3) the substrate temperature during deposition, (4) the oxygen pressure during deposition, (5) the total deposition time and corresponding film thickness, and (6) the postdeposition cooling rate and oxygen pressure. Based on the deposition conditions given in Refs. 5 and 6, a total of 100 deposition runs were undertaken in order to provide a systematic scan over the parameters listed above. The objective was to determine the optimum conditions to realize films with the lowest possible microwave loss. For each deposition run, the FMR linewidth was measured at 9.5 GHz for perpendicular-to-plane (PTP) and in-plane (IP) applied field configurations. For the films with the lowest linewidths, AFM surface scan images were obtained and the cubic structure and the orientation dispersion were examined by x-ray diffraction.

The sequence of depositions described above led to a determination of optimum conditions for low linewidth films. These conditions are listed in Table I. These conditions gave films with thicknesses in the 0.7–1.0-μm range. Longer deposition times produced thicker films, but these tended to separate from the substrate. Presumably, this is due to the remaining lattice mismatch between the LiZn-ferrite and the MgO substrate and the increasing stress as the films grow thicker. The best films had extremely smooth surfaces. The AFM imaging gave a local surface roughness of about 0.26 nm. These optimized films had a 9.5-GHz half power FMR linewidths of about 57 Oe. Crystallographic and microwave properties are considered in detail below.

III. FILM CHARACTERIZATION AND STATIC MAGNETIC PROPERTIES

The room-temperature crystallographic data provide clear and conclusive evidence of good epitaxial film quality and cubic structure. Standard $\theta/2\theta$ source and detector scans were used to verify the cubic structure. The (004) LiZnF diffraction line was then used for a rocking curve measurement to determine the normal axis angular dispersion. Finally, (115)-plane diffraction lines and sample rotation were used to check the cubic fourfold symmetry. The Miller indices used here reference the film plane as (001).

Figure 2 shows the representative XRD results for one particular 0.70-μm-thick film obtained for the optimum PLD parameters listed above. Graph (a) shows a standard $\theta/2\theta$ diffraction scan, with the XRD intensity shown on the vertical axis. The film was oriented such that the θ rotation gave a scattered beam that matched the specular reflection from the surface and all detected peaks come from reciprocal-lattice vectors normal to the film plane. The range of angles from 46° to 91° is abbreviated with the broken line and the other parts are magnified. The lines associated with the MgO substrate and the LiZnF film, as well as those for the copper XRD source, are identified in the diagram. There are two LiZnF (008) lines, one for each of the two Cu $K\alpha$ source frequencies. The main graph in (b) shows a rocking curve for

Downloaded 07 Jul 2005 to 129.82.140.121. Redistribution subject to AIP license or copyright, see http://jap.aip.org/jap/copyright.jsp

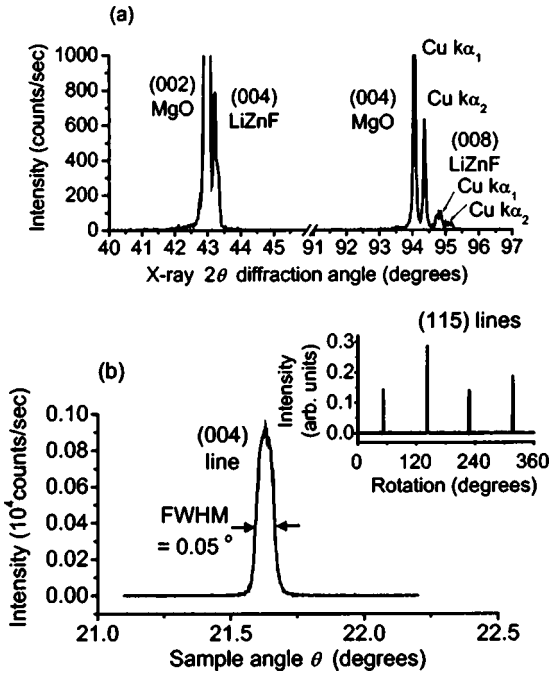

FIG. 2. X-ray diffraction (XRD) data for the 0.70-μm-thick LiZn-ferrite film. Graph (a) shows a standard $\theta/2\theta$ XRD intensity scan. The sample orientation was such that the θ rotation matched the scattered beam to the specular reflection from the surface. The identified diffraction peaks are as indicated. The main graph in (b) shows a rocking curve for the (004)-LiZnF diffraction line with a full width at half maximum of 0.05°. The inset in (b) shows the XRD intensity vs in-plane rotation angle, with the $\theta/2\theta$ angles and sample tilt set to detect the diffraction from the (115) LiZnF lattice planes.

the (004) LiZnF peak in (a). The inset in (b) shows the XRD intensity versus the in-plane sample rotation angle about the film normal for the (115) diffraction line. For this measurement, the $\theta/2\theta$ angles and sample tilt were set to detect the diffraction from the (115) LiZnF lattice planes and the sample was rotated to check the fourfold symmetry over the full area of the film.

The data in (a) show the expected (001)-plane diffraction peaks for a single-crystal (001)-plane-oriented LiZn-ferrite film. Except for the MgO lines, there are no additional diffraction peaks in the spectra. Note that the LiZnF peaks are for a lattice parameter that is twice that for the MgO substrate. The LiZn-ferrite peaks show that the material is in a single phase and has a very good epitaxial orientation. The full width at half maximum of the XRD rocking curve in (b) is 0.05°, and this width provides a quantitative measure of the *c*-axis dispersion. This small orientation dispersion provides further evidence that the film is epitaxial. The full 0°–360° angle scan in the graph (b) inset provides a further demonstration that the epitaxy is texture-free over the entire 3 mm^2 probe beam area. The graph shows clear fourfold symmetry and very sharp peaks for the azimuthal in-plane angle scan over the (115)-plane diffraction lines. These XRD data are in significant contrast with the results in Ref. 5, which showed peak widths of about 20°, evidence of a strong lattice mismatch, and significant texturing.

Figure 3 shows a representative AFM surface image for the same film. The selected area was 1×1 μm^2. The vertical color scale range is 5 nm. The change of color over the

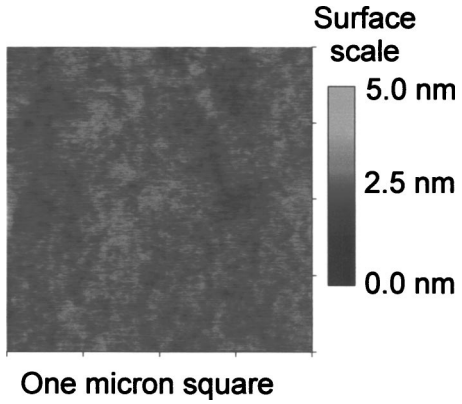

FIG. 3. Representative atomic force microscopy (AFM) surface scan image for the optimum linewidth 0.70-μm-thick LiZn-ferrite film. The image was taken over a 1-μm square area and with a vertical scale range of 5 nm. The vertical color scale is as indicated.

image indicates the short-range thickness variations of about 0.3 nm or so. The actual root-mean-square (rms) surface roughness is about 0.25 nm over a given 1-μm scan length. This rms roughness is quite small. Based on the LiZnF lattice parameter of 8.33 Å, this roughness corresponds to about one-third of the unit-cell layers. It is important to note that surface roughness is a critical parameter for the realization of low FMR linewidths in ferrite films. A very smooth surface, therefore, is also one prerequisite for low microwave loss.

The room-temperature static magnetization M was measured as a function of the static external applied field H by vibrating sample magnetometry. The data were obtained for PTP[001] and IP[100] applied field directions, both of which are "hard" magnetocrystalline directions. For a negative cubic magnetocrystalline anisotropy, as in Li-ferrite single-crystal materials, the [111] directions are easy direction and all [100] directions are hard. Figure 4 shows the representative data on the magnetic induction $4\pi M$ vs H data for the same 0.70-μm-thick film used for the x-ray analysis in Fig. 2. The graph shows the results for both the PTP and the IP field configurations, as indicated. The lines connecting the data points show simple spline fits. The data are shown for fields up to 10 kOe.

The IP hysteresis loop is relatively narrow and fairly square, with a coercive force of about 25 Oe and quasisaturation at applied fields above 1.6 kOe or so. The slope of the high-field IP $4\pi M(H)$ response is about 0.4 kG/kOe. The

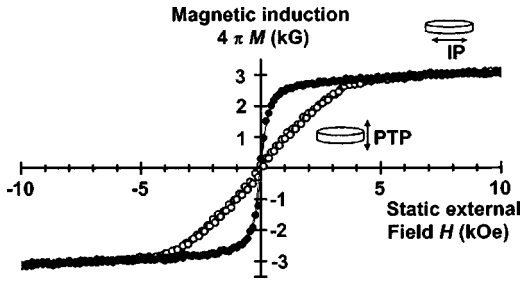

FIG. 4. Magnetic induction $4\pi M$ vs static external magnetic field H for the 0.70-μm-thick film. The field was applied perpendicular-to-plane (PTP) or in-plane (IP), as indicated. The points show the data and the lines show spline fits to the data.

Downloaded 07 Jul 2005 to 129.82.140.121. Redistribution subject to AIP license or copyright, see http://jap.aip.org/jap/copyright.jsp

PTP data show a linear change with field above 5 kOe or so that matches the IP response. These data sets give a $4\pi M$ value of about 3.1 kG at $H=10$ kOe. For 0–3-kOe fields or so, the PTP response is linear in field and has a slope of about 0.78 kG/kOe. The intercept field point between the low-field linear PTP data and the common high-field responses is at about 3.6 kOe. The extrapolated zero-field magnetic induction $4\pi M_{S0}$, obtained from the linear high-field $4\pi M(H)$ IP and PTP responses, is 2.73 kG.

The hysteresis loop data are consistent with the known properties of LiZnF materials. The small coercive force for the IP hysteresis loop is related to the domain-wall motion and is one indication of good single-crystal film quality. The rounded top part of the IP hysteresis loop is related to the magnetocrystalline anisotropy and domain rotation into the hard in-plane direction. The film $4\pi M$ value at 10 kOe is somewhat lower than the 8-kOe $4\pi M$ value of 3.5 kG, as shown in Fig. 1 for $x=0.6$. The nonzero slope of the high-field response and the lack of clear saturation can be attributed to the noncollinear spin structure and canting[1,4] and the 0.4-kG/kOe slope of the high-field response for both configurations. The PTP/IP intercept point at value of 3.6 kOe likely represents a combination of the thin-film demagnetizing field of $4\pi M$ and anisotropy. From the data, this anisotropy, composed of both magnetocrystalline and stress-induced terms, does not exceed a few hundred Oe. Anisotropy is considered in more detail below. It is noteworthy, however, that the zero-field extrapolated $4\pi M_{S0}$ value is close to literature $4\pi M_S$ values for bulk single crystals that lie in the 2.8-kG range.[2] Taken together, the crystallographic results and the static magnetic data show that these PLD films (1) have a cubic structure, (2) are (001) plane oriented with very little dispersion or texture, (3) have a very smooth surface, and (4) have $4\pi M$ values that are consistent with but perhaps slightly less than those found for bulk LiZn-ferrite. Section IV will show that these films also have exceptional microwave properties which are much better than previous reports.

IV. FERROMAGNETIC-RESONANCE RESULTS AND ANALYSIS

A. Ferromagnetic-resonance data

Ferromagnetic-resonance absorption versus static field curves were measured at a nominal frequency of 9.5 GHz for the PTP field configuration, with the field along the perpendicular [001] crystallographic direction, and the IP field configuration, with the in-plane field at some angle ϕ relative to the in-plane [100] direction. The actual data consisted of the derivative profiles obtained by a standard field-swept shorted waveguide technique. The results shown below are for the same 0.70-μm-thick film sample used for the results in Figs. 2–4.

Figure 5 shows a typical result for the derivative of the absorbed power versus static external field H for the main resonance. These particular data are for the PTP configuration. The resonance field position is 6.493 kOe. The vertical-dashed lines delineate the negative to positive peak separation of 33 Oe that defines the derivative linewidth. For a Lorentzian line shape, this value would correspond to a half power linewidth of $33\sqrt{3}$, or 57 Oe. The data show, however, that the FMR mode response is distorted on the low-field side and is not strictly symmetric. This distortion is likely due to a broad adjacent mode somewhat below the main resonance in field.

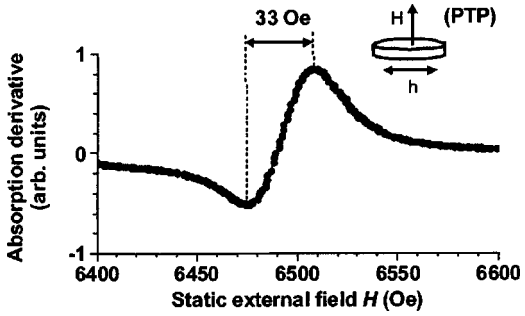

FIG. 5. Representative the absorption derivative vs static external field H profile at 9.5 GHz for the same 0.70-μm-thick film sample used for the results in Figs. 2–4. The inset indicates the field geometry, with a perpendicular-to-plane static field H and an in-plane microwave field h for the PTP configuration. The vertical-dashed lines and the 33-Oe label indicate the usual "derivative" linewidth.

Figure 6 shows the representative IP data on the FMR center field position H_{res} as function of the in-plane resonance field angel ϕ relative to [100]. The solid circles show the data. The solid curve shows a fit to the standard uniform mode FMR response equations that will be discussed in Sec. IV B. The principal crystallographic directions are also indicated. These data show clearly the in-plane cubic anisotropy of the film and the match to the cubic anisotropy of the MgO substrate. Note that the [100] direction corresponds to a hard anisotropy axis. This is consistent with the established negative first-order anisotropy energy parameter K_1 and easy [111] direction for lithium ferrite.

The linewidths for the IP field configuration are about a factor of two larger than PTP linewidths. This increase can be attributed to two magnon scattering. It provides an indication of imperfections and inhomogeneities in the film.[11] These IP linewidths, however, show no significant angular dependence. This indicates that the inhomogeneities are not related to crystallographic morphology. This is in contrast

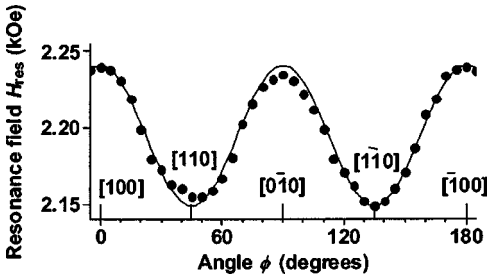

FIG. 6. Resonance field H_{res} as a function of the in-plane field angle ϕ relative to the in-plane [100] crystallographic direction for the same (001) 0.70-μm-thick film sample used for the results in Figs. 2–5. The solid circles show the data and the solid curve shows a computed response based on the uniform mode FMR response for a (001) thin film with cubic anisotropy and a negative first-order anisotropy constant as discussed in Sec. IV B. The principal in-plane directions are indicated along the horizontal axis.

Downloaded 07 Jul 2005 to 129.82.140.121. Redistribution subject to AIP license or copyright, see http://jap.aip.org/jap/copyright.jsp

with a recent work on single-crystal iron films in which the cubic texture produces a significant linewidth variation with the in-plane field angle ϕ.[12]

B. FMR field analysis and fits for cubic anisotropy

The FMR field data were analyzed in terms of the standard uniform mode FMR theory for thin films with cubic anisotropy.[13,14] Consider a [001] film with a negative first-order magnetocrystalline anisotropy constant K_1, a saturation magnetization M_s, and an anisotropy field parameter $H_A = 2|K_1|/M_s$. In terms of these parameters, the PTP and IP FMR field frequency connections, for fields sufficiently large to bring the vector magnetization into alignment or near alignment with the applied field, can be written as

$$\omega = |\gamma|(H_{\text{res}} - 4\pi M_s - H_A) \quad \text{(PTP)} \tag{1}$$

and

$$\omega = |\gamma| \sqrt{\left[H_{\text{res}} + 4\pi M_s - \frac{1}{2}H_A(1 + \cos^2 2\phi)\right] \cdot [H_{\text{res}} - H_A \cos 4\phi]} \quad \text{(IP)}. \tag{2}$$

In the above, ω denotes the excitation frequency and γ is the electron gyromagnetic ratio. Note that γ is negative for electrons.

Keep in mind that the above equations are specific to thin films with cubic magnetocrystalline anisotropy, a negative K_1, and a (001)-plane films. The anisotropy field parameter H_A is taken as positive. Based on the above equations, fits to the PTP and the IP resonance field position data were used to obtain FMR determinations of the nominal saturation induction $4\pi M_s$ and anisotropy field H_A for the film. For these fits, $|\gamma|/2\pi$ was set at the free-electron value of 2.8 GHz/kOe. For $4\pi M_s = 3.123$ kG and $H_A = 59$ Oe, one could fit the experimental H_{res} for the PTP geometry and obtain the solid curve shown in Fig. 6 for $H_{\text{res}}(\phi)$.

This fitted $4\pi M_s$ value is reasonably consistent with the vibrating-sample magnetometer (VSM) results presented above. The fitted anisotropy field is somewhat larger than published literature values for bulk lithium ferrite materials. The implicit K_1 value from the $4\pi M_s$ and H_A values given above is -7.33×10^3 ergs/cm^3. This is about a factor of five smaller than the reported K_1 values for bulk lithium zinc ferrite. The $H_{\text{res}}(\phi)$ response in Fig. 6 is unambiguous and the fit to a cubic response function is also quite good. This indicates that the $H_A = 59$ Oe for the present heavily Zn-substituted lithium ferrite film is reasonably accurate.

In spite of the convincing XRD evidence for the good epitaxy and single crystallinity for the film, it may also be noteworthy that the FMR linewidths are of the same order as the anisotropy field. The linewidths, while smaller than ever obtained before for PLD lithium ferrite films, are still much larger than the values reported for bulk lithium ferrite single crystals.

V. SUMMARY

High-quality single-crystal lithium ferrite films have been fabricated on MgO substrates by pulsed laser deposition. The key consideration in the growth of high-quality films was in the use of a zinc-doped target material with a larger lattice parameter than pure lithium ferrite. The XRD data indicate a very good single-crystal texture-free structure without impurities and the AFM data show smooth surfaces. The 9.5-GHz half power ferromagnetic-resonance main mode linewidth for the best films was 57 Oe. This linewidth is six times smaller than the previous reports. From the VSM and FMR data, the film saturation magnetic induction is about 3 kG, in reasonable agreement with bulk values. The FMR data also show a clear cubic anisotropy with an H_A value of 59 Oe. The corresponding first-order anisotropy energy constant K_1 is about five times larger than that found for bulk lithium zinc ferrite.

ACKNOWLEDGMENTS

This work was sponsored in part by the Office of Naval Research under Grant Nos. N00014-94-1-0096 and N00014-03-1-0070, and the National Science Foundation under Grant Nos. DMR-9801649 and DMR-0108797. Advice and assistance from Dr. Vincent Harris, previously of the Naval Research Laboratory and now at Northeastern University, are gratefully acknowledged.

[1] G. O. White and C. E. Patton, J. Magn. Magn. Mater. **9**, 299 (1978).
[2] W. H. Von Aulock, *Handbook of Microwave Ferrite Materials* (Academic, New York, 1965).
[3] C. E. Patton, C. A. Edmondson, and Y. H. Liu, J. Appl. Phys. **53**, 2431 (1982).
[4] C. E. Patton and Y. H. Liu, J. Phys. C **16**, 5995 (1983).
[5] S. A. Oliver, C. Vittoria, G. Balestrino, S. Martellucci, G. Petrocelli, A. Tebano, and P. Paroli IEEE Trans. Magn. **30**, 4933 (1994).
[6] G. Balestrino, S. Martellucci, A. Paoletti, P. Paroli, G. Petrocelli, A. Tebano, S. A. Oliver, and C. Vittoria, Solid State Commun. **96**, 997 (1995).
[7] E. G. Spencer, D. A. Lepore, and J. W. Nielsen, J. Appl. Phys. **39**, 732 (1968).
[8] G. A. Petrokovskii and V. N. Berzhanskii, Sov. Phys. Solid State **13**, 495 (1971).
[9] Y. Y. Song, S. Kalarickal, and C. E. Patton, J. Appl. Phys. **94**, 5103 (2003).
[10] P. B. Braun, Nature (London) **170**, 1123 (1952).
[11] M. Sparks, *Ferromagnetic Relaxation Theory* (McGraw-Hill, New York, 1965).
[12] G. Woltersdorf and B. Heinrich, Phys. Rev. B **69**, 184417 (2004).
[13] M. Marysko, Czech. J. Phys., Sect. B **31**, 1187 (1981).
[14] Y. Zhai *et al.*, J. Appl. Phys. **93**, 7622 (2003).
[15] C. A. Edmondson and C. E. Patton (unpublished).

Downloaded 07 Jul 2005 to 129.82.140.121. Redistribution subject to AIP license or copyright, see http://jap.aip.org/jap/copyright.jsp